Large amplitude dynamics of micro/nanomechanical resonators actuated with electrostatic pulses

J. Juillard[1], A. Bonnoit[1], E. Avignon[1], S. Hentz[2], E. Colinet[2]
[1]SSE-SUPELEC, Gif-sur-Yvette, France, jerome.juillard@supelec.fr
[2]CEA-LETI, MINATEC, Grenoble, France, sebastien.hentz@cea.fr

Abstract. In the field of resonant NEMS design, it is a common misconception that large-amplitude motion, and thus large signal-to-noise ratio, can only be achieved at the risk of oscillator instability. In the present paper, we show that very simple closed-loop control schemes can be used to achieve stable large-amplitude motion of a resonant structure, even when jump resonance (caused by electrostatic softening or Duffing hardening) is present in its frequency response. We focus on the case of a resonant accelerometer sensing cell, consisting in a nonlinear clamped-clamped beam with electrostatic actuation and detection, maintained in an oscillation state with pulses of electrostatic force that are delivered whenever the detected signal (the position of the beam) crosses zero. We show that the proposed feedback scheme ensures the stability of the motion of the beam much beyond the critical Duffing amplitude and that, if the parameters of the beam are correctly chosen, one can achieve almost full-gap travel range without incurring electrostatic pull-in. These results are illustrated and validated with transient simulations of the nonlinear closed-loop system.

1. Introduction

Resonant sensing consists in measuring the frequency shift of a system subject to the variation of a given physical quantity. Because of its moderate complexity, this measurement technique is becoming commonplace in the context of MEMS and NEMS devices [1-3]. This paper focuses on closed-loop resonant sensors, where the micromechanical structure is brought to oscillate by being placed inside a feedback loop [4-6]. In the present work, the structure is a clamped-clamped beam, the motion of which is sensed capacitively. It is maintained in an oscillation state with pulses of electrostatic force that are delivered whenever the detected signal (the position of the beam) crosses zero [7-8]. In order to maximize the signal-to-noise ratio (SNR) and, thus, to relax the constraints on the electronic design, the detected signal must be as large as possible, which means that, for a given set of structural parameters and a given bias voltage, the oscillation amplitude of the resonant beam must also be as large as possible. This raises questions concerning what oscillation amplitude can be sustained without incurring mechanical [9-10] or electrostatic [11-12] instability.

We show in this paper that, in spite of the nonlinearities, the proposed feedback scheme ensures the stability of the motion of the beam much beyond the critical Duffing amplitude. We also show that, if the parameters of the beam are correctly chosen, one can realistically achieve almost full-gap travel range without incurring electrostatic pull-in.

In section 2, the sensing cell of the resonant accelerometer that is the basis of our work is briefly described. The focus is brought on the capacitive detection and actuation schemes. In section 3, a simplified one-degree-of-freedom (1-DOF) model of the beam is derived. In particular, an approximate expression of the first modal component of the electrostatic force acting on the beam is determined. In section 4, the electrostatic instabilities that are inherent to the design are addressed. We show, using the model of section 3, that it is possible to achieve almost full-gap travel range without pull-in if the bias voltage is correctly chosen. In section 5, describing function analysis (DFA) is used to characterize the oscillations of the closed-loop system. We show that, when the electrostatic pulses are short with respect to the natural period of the system, there exists a unique oscillation regime and that it is stable, provided the condition for electrostatic stability established in section 3 is met. These results are illustrated in section 6 and validated with transient simulations of the closed-loop system.

2. Framework

2.1 Sensing principle

The accelerometer consists in a suspended seismic mass, which is anchored to the substrate via a short beam acting as a flexure. A longer, more flexible beam, perpendicular to the flexure, acts as a sensing element (figure 1). When the mass is subject to acceleration, the sensing beam undergoes compressive or tensile stress (depending on the direction of the acceleration), resulting in a variation of its stiffness. This variation can then be detected via a shift $\Delta\omega$ of its natural pulsation ω_0.

Two sensing principles may be used to monitor frequency shifts. In open-loop sensing, the structure is excited using a repeated chirp (a sine wave with slowly increasing or decreasing frequency). The frequency response of the structure can then be calculated and the value of the "open-loop resonance frequency" (the frequency for which the frequency response is maximal) can then be determined and monitored. In closed-loop sensing, the micromechanical structure is placed inside a feedback loop, without external input. If the feedback loop is correctly designed, the structure starts oscillating at a so-called "closed-loop resonance frequency", which shifts along with the natural frequency of the structure. The practical advantage of closed-loop sensing compared to open-loop sensing is that it only requires frequency measurements, which can be performed by counting the rate of zero-crossings of the electrical signals in the feedback loop (this typically requires one comparator and a time reference). On the other hand, open-loop sensing requires measuring the amplitude of motion of the resonant element. In an application where the sensing cell is co-integrated with its electronics, open-loop sensing (which involves high-resolution A/D and D/A converters for signal generation and measurement) entails a greater cost than closed-loop sensing. From a mathematical point of view, closed-loop sensors are autonomous systems, whereas open-loop sensors are non-autonomous. The accelerometer sensing cell considered in the present paper is operated in closed-loop.

2.2. Description of the accelerometer sensing cell

In the ANR-funded M&NEMS project, which sets the framework of this paper [8], the sensing beam is placed between two equidistant electrodes, so as to be the midpoint of a capacitive half-bridge. The transmission line and contact pads between the structure and the control electronics give rise to a parasitic capacitance C_p, typically on the order of several pF, which is much larger than the nominal capacitance of the structure (on the order of 1fF) and leads to poor SNR [13]. At the output of the charge amplifier, the voltage V_{out} can be written:

$$V_{out} = \frac{K}{C_p + (1+K)C_f} Q_e + V_{offset}, \qquad (1)$$

where Q_e is the charge accumulated on the mobile beam, K is the gain of the operational amplifier, C_f is the feedback capacitance and V_{offset} is an integration constant that is removed with high-pass filtering. We may then assume throughout the rest of the paper that $V_{offset} = 0$ and that $Q_e = 0$ when the beam is halfway between the electrodes, so that $V_{out} = 0$ when the displacement of the beam w is uniformly 0.

In order to maximize the SNR, the detected signal must be as large as possible, which means that, for a given set of structural parameters and a given bias voltage, the oscillation amplitude of the resonant beam must also be as large as possible. We show in what follows that such large-amplitude motion may be sustained without incurring mechanical or electrostatic instability, if a proper feedback scheme is used to actuate the beam.

2.3. Actuation and detection schemes

Applying brief negative or positive pulses of electrostatic force to the beam whenever it passes through a certain reference position (typically $V_{out} = w = 0$) can bring the system into a sustained self-oscillation state [7-8]. The voltage pulses (with amplitude $\pm V_p$ and duration $T_p << 2\pi/\omega_0$) can be delivered to the central electrode, as in [7], or through the biasing electrodes (figure 1). Both solutions are equivalent from a dynamical system point of view. In either case, provided the length L and width b of the beam are large with respect to G, the electrostatic gap, one may consider that every slice of area bdx of the beam is subject to an electrostatic force $F_e dx$, where lineic density F_e is given by the plane capacitance approximation:

$$F_e = \frac{\varepsilon_0 b}{2}\left(\frac{(V_b/2 - V_c)^2}{(G-w)^2} - \frac{(V_b/2 + V_c)^2}{(G+w)^2}\right) = \frac{2\varepsilon_0 b}{\left(G^2 - w^2\right)^2}\left(\frac{V_b}{2}w - V_c G\right)\left(\frac{V_b}{2}G - V_c w\right), \qquad (2)$$

where ε_0 is the permittivity of vacuum, V_b is the bias voltage and V_c is the control voltage (i.e. the voltage applied to the mobile beam). Under the same assumptions, the lineic charge density accumulated on an elementary slice of the beam is:

$$\sigma_e = \varepsilon_0 b\left(\frac{-V_b/2 + V_c}{G-w} + \frac{V_b/2 + V_c}{G+w}\right) = \varepsilon_0 b\left(2V_c\frac{G}{G^2 - w^2} - V_b\frac{w}{G^2 - w^2}\right), \qquad (3)$$

When no pulse is being delivered to the beam, $V_c = 0$ and (2) and (3) simplify to:

$$F_e = F_{soft} = \frac{\varepsilon_0 b G V_b^{\,2}}{2}\frac{w}{\left(G^2 - w^2\right)^2}, \qquad (4)$$

which corresponds to the electrostatic softening of the system, and

$$\sigma_e = -\varepsilon_0 b V_b \frac{w}{G^2 - w^2}. \qquad (5)$$

Note that (4) and (5) vanish when w is uniformly 0 or, assuming that the deformation of the beam is unimodal, when $V_{out} = 0$.

Since the pulses are very short, there is only a very small amount of crosstalk between the actuation and detection schemes. Assimilating these finite pulses to ideal Dirac pulses, one may then consider that (4) and (5) are always valid except at instants t_0 when V_{out} is exactly zero, in which case:

$$\lim_{\tau\to 0}\int_{t_0-\tau}^{t_0+\tau} F_e\,dt = \pm\frac{\varepsilon_0 b}{G^2}V_b V_p T_p \qquad (6)^1$$

and

$$\lim_{\tau\to 0}\int_{t_0-\tau}^{t_0+\tau} \sigma_e\,dt = \mp\frac{2\varepsilon_0 b}{G}V_p T_p\,. \qquad (7)$$

The fact that, in practice, the pulses have finite duration is not detrimental to the proper functioning of the system, because when the self-oscillation conditions are met, voltage pulses are delivered in such a way that they do not modify the sign of V_{out} [7]. In other words, the sign of V_{out} is always the exact opposite as the sign of the displacement of the beam, even during the voltage pulses. This makes the design of the electronic feedback loop very simple: basically, all it takes to generate voltage pulses when $w=0$ is a comparator and a pair of monostable multivibrators.

Assuming the electrodes have the same length and width as the beam, the system is governed by:

$$\frac{Ebh^3}{12}\frac{\partial^4 w}{\partial x^4} - T\frac{\partial^2 w}{\partial x^2} - \frac{\varepsilon_0 b G V_b{}^2}{2}\frac{w}{\left(G^2-w^2\right)^2} + \mu\frac{\partial w}{\partial t} + \rho bh\frac{\partial^2 w}{\partial t^2} = F_{pulse} \quad (8),$$

where E is Young's modulus, ρ is the density, h is the thickness of the beam, μ is a linear damping coefficient, T is the axial force caused by the elongation of the beam:

$$T = \frac{Ebh}{2L}\int_0^L\left(\frac{\partial w}{\partial x}\right)^2 dx\,. \qquad (9)$$

$F_{pulse} = F_e - F_{soft}$ is the "pulsed" component of the electrostatic force and consists of Dirac pulses occurring when $V_{out}=0$, with amplitudes given by (6). In the next section, we define the pull-in voltage of the structure and its pull-in amplitude and show that, with proper design, one can use pulse-actuation to achieve almost full-gap travel range.

3. Model derivation

In the context of a resonant sensor application, it is a reasonable to assume that the deformation of the beam is unimodal. Let us then write $\tilde{w}(\tilde{x},\tilde{t}) = a(\tilde{t})w_0(\tilde{x})$, where w_0 is the first clamped-clamped beam eigenmode, with eigenvalue $\beta_0{}^4$ ($\beta_0 \approx 4.730$) and where the following dimensionless quantities are used: $\tilde{w} = w/G$, $\tilde{x} = x/L$ and $\tilde{t} = \omega_0 t$,

$$\omega_0 = \frac{\beta_0{}^2}{\sqrt{12}}\frac{h}{L^2}\sqrt{\frac{E}{\rho}} \approx 6.459\frac{h}{L^2}\sqrt{\frac{E}{\rho}}\,. \qquad (10)$$

The value of $w_0(1/2)$ is set to 1, so that $a=\pm 1$ corresponds to full-gap displacement of the midpoint of the beam. Projecting (8) on w_0, we obtain the following model of the beam dynamics:

$$a\left[1+\gamma a^2 - \delta I(a)\right] + \frac{\dot{a}}{Q} + \ddot{a} = f_p\Delta(a,\dot{a}), \quad (11)$$

---

[1] The terms involving $V_c{}^2$ in (2) are cancelled out because the pulses are delivered when $w=0$. Thus, the amplitude of the actuation is proportional to V_p, regardless of whether $V_p << V_b$.

where $\Delta(a,\dot{a})$ designates a Dirac pulse occurring when $a=0$, with the same sign as $\dot{a}$ (giving the oscillator a kick in the direction of its motion),

$$\gamma = \frac{G^2}{h^2}\frac{6}{{\beta_0}^4}\left(\int_0^1\left(\frac{\partial w_0}{\partial \tilde{x}}\right)^2 d\tilde{x}\right)^2 \Bigg/ \left(\int_0^1 {w_0}^2 d\tilde{x}\right) \approx 0.719\frac{G^2}{h^2}, \quad (12)$$

$$\delta = \frac{{V_b}^2}{{V_{pi}}^2},\ V_{pi} = \frac{{\beta_0}^2}{\sqrt{6}}\left(\frac{Eh^3G^3}{\varepsilon_0 L^4}\right)^{1/2} \approx 9.134\left(\frac{Eh^3G^3}{\varepsilon_0 L^4}\right)^{1/2}, \quad (13)$$

$$I(a) = \left(\int_0^1 \frac{{w_0}^2}{\left(1-a^2{w_0}^2\right)^2} d\tilde{x}\right) \Bigg/ \left(\int_0^1 {w_0}^2 d\tilde{x}\right), \quad (14)$$

$$f_p = 2\frac{V_b V_p}{{V_{pi}}^2}\tau_p \left(\int_0^1 w_0 d\tilde{x}\right) \Bigg/ \left(\int_0^1 {w_0}^2 d\tilde{x}\right) \approx 2.639\frac{V_b V_p}{{V_{pi}}^2}\tau_p, \quad (15)$$

where $\tau_p = \omega_0 T_p$ and Q is the quality factor of the system. There exists no closed-form expression of $I(a)$, however it is possible to approximate it with:

$$I(a) \approx \hat{I}(a) = \left(1-a^2\right)^{-3/2}, \quad (16)$$

as is explained in Appendix A. The relative error between $I(a)$ and $\hat{I}(a)$ is less than 5% across the whole gap - it can even be reduced to less than 1% by multiplying $\hat{I}(a)$ with $\left(1-0.041a^2\right)$ (see Appendix A). Because of its range of validity, this approach is better suited to large amplitude dynamics than Taylor series expansion, which is commonly used in MEMS/NEMS modeling. In particular, it allows us to capture the dynamic pull-in behavior of a pulse-actuated in a simple way, as is shown in section 4.

4. Pull-in phenomena

A fundamental limit to the displacement amplitude of electrostatically-actuated devices is set by the static pull-in phenomenon [11-12]. The pull-in amplitude is classically determined as the displacement amplitude for which the electrostatic softening force and the mechanical restoring force are balanced but the equilibrium is unstable. In the case of the clamped-clamped beam setup of figure 1, it is clear that, in the absence of (pulsed) actuation forces, $w=0$ is always an equilibrium point and that, provided V_b is small enough, this equilibrium point is stable.

The threshold value of V_b beyond which this equilibrium becomes unstable is determined in sub-section 4.1. We then show in sub-section 4.2 that the electrostatic nonlinearity sets an upper bound to the oscillation amplitude of the structure and determine this limit.

4.1. Determination of the static pull-in voltage

The problem of the beam at rest subject to an increasing bias voltage is similar to the problem of a beam subject to increasing compressive stress: the beam is gradually softened until a critical point is reached for which it is pulled-in (or it buckles, in the mechanical analogy). As in classic Euler buckling problems [14], the equilibrium position ($w=0$) becomes unstable when the first eigenvalue of the linearized spatial partial differential operator appearing in (8) equals zero. In other words, the beam is pulled-in from its central position when the linearized modal stiffness of the system equals zero. From (11), the modal stiffness is $1+\gamma a^2-\delta I(a)$. Linearizing this expression for $a=0$ yields the following pull-in condition:

$$\delta = 1, \quad (17)$$

i.e. $V_b = \pm V_{pi}$. Working with $\delta<1$ ensures only that $w=0$ is a stable equilibrium point around which the beam can oscillate. In the following sub-section, we show that there exists a maximal displacement amplitude beyond which the beam is pulled-in to one of the electrodes and that this amplitude depends on V_b.

4.2. Determination of the maximal displacement amplitude

The first term on the left-hand side of (11) corresponds to the restoring forces acting on the beam, including the linear elastic and nonlinear elastic and electrostatic components, which derive from a potential energy E_{pot}. Using (16), E_{pot} can be expressed as:

$$E_{pot} = \frac{1}{2}a^2 + \frac{1}{4}\gamma a^4 - \delta\frac{1}{\sqrt{1-a^2}}. \qquad (18)$$

E_{pot} is represented in figure 2 for different values of δ and γ.

When $\delta < 1$, the central position is stable, as shown in sub-section 4.1. E_{pot} is maximal when:

$$1 + \gamma a^2 - \delta\left(1-a^2\right)^{-3/2} = 0, \qquad (19)$$

which has two solutions $\pm a_{\max}$ ($a_{\max} > 0$), both of which correspond to unstable equilibria. Now, let us suppose that energy is injected into the system (initially at rest) whenever $a = 0$, in the form of short electrostatic pulses, so that an oscillation starts building up. If too much energy is injected into the system, it moves past the potential barrier in $\pm a_{\max}$ and the beam is inevitably pulled-in to one of the electrodes. Otherwise, it eventually reaches a steady-state regime and stabilizes at an amplitude which is inferior to $a_{\max}$. Thus $a_{\max}$ is the maximal displacement amplitude that can be achieved by an oscillating pulse-actuated clamped-clamped beam without incurring pull-in.

When $\gamma = 0$, the following analytical expression can be derived from (19):

$$a_{\max} = \sqrt{1-\delta^{2/3}}. \qquad (20)$$

Accounting for stiffening results in a larger value of $a_{\max}$ than predicted by (20) (figure 3), however no analytical expression of $a_{\max}$ can be found. It is notable that very small values of δ result in $a_{\max}$ being very close to 1.

$\delta \geq 1$ corresponds to the case when the central position is unstable (figure 2). However, the fact that the beam is "pulled-in" does not mean it necessarily comes in contact with an electrode: it might instead get stuck in one of the potential wells that appear for large values of γ. In this configuration, it should also possible to use a pulse-actuation scheme to achieve stable oscillations around $a = 0$ even though the central position is intrinsically unstable.

In the following section, we assume that $\delta < 1$.

5. Analysis of the closed-loop system

Describing function analysis, or equivalent linearization, is a method used (mostly) by engineers to determine certain properties of weakly nonlinear systems subject to various stimuli. When the only stimuli are sine waves, the method is also known as harmonic balance, in which case it yields the same results as those one would obtain through the method of averaging (or KBM method) [15] used to first order. In this context, the difference between the two methods is purely a matter of perspective, the describing function formalism being more oriented toward the design of control systems.

5.1. Describing function analysis of the closed-loop system

An equivalent block-diagram representation of (11) is shown in figure 4. One may consider the closed-loop system as a linear system with a triple feedback nonlinearity. If the "filter hypothesis" holds (i.e. if the linear part efficiently filters out the high-order harmonic content output by the nonlinearity), one may apply DFA to the system and expect good qualitative and quantitative results [15]. DFA is then particularly well-suited to the case of a resonant structure with a large quality factor oscillating with a pulsation close to ω_0.

The existence of a periodic regime, and its characteristics (amplitude, pulsation and stability) can then be determined by:

1. assuming $a = A\sin(\omega t)$, $0 < A < 1$, $\omega > 0$

2. finding the equivalent complex gain $N(A,\omega)$ of the nonlinear part $F(a,\dot{a})$,

$$N(A,\omega)=\frac{\omega}{\pi A}\int_0^{2\pi/\omega}F(a,\dot{a})\exp(j\omega t)dt \qquad (21)$$

3. checking for an oscillatory regime satisfying the Barkhausen condition, i.e. solving for the limit cycle amplitude A_{osc} and pulsation ω_{osc}

$$N(A,\omega)H(j\omega)+1=0 \quad (22)$$

where $H(j\omega)$ is the transfer function of the linear part.

(22) can be split in two equations and rewritten as

$$\mathrm{Re}(A,\omega)=\mathrm{Im}(A,\omega)=0 \quad (23)$$

where Re and Im are the real and imaginary part of $N(A,\omega)+1/H(j\omega)$.

Step 3 is equivalent to imposing that the total phase lag in the loop is equal to zero. An oscillatory regime defined by (22-23) is stable with respect to slight perturbations if the following inequality is satisfied:

$$\frac{\partial \mathrm{Re}}{\partial A}\frac{\partial \mathrm{Im}}{\partial \omega}-\frac{\partial \mathrm{Im}}{\partial A}\frac{\partial \mathrm{Re}}{\partial \omega}>0, \qquad (24)$$

where the partial derivatives are taken at $A=A_{osc}$ and $\omega=\omega_{osc}$.

4.2. Determination of $N(A,\omega)$

The nonlinear feedback block consists in three nonlinearities in parallel. Their equivalent complex gain is then given by:

$$N(A,\omega)=N_{Duff}(A)+N_{soft}(A)+N_{pulse}(A,\omega), \qquad (25)$$

where $N_{Duff}(A)$, $N_{soft}(A)$ and $N_{pulse}(A,\omega)$ are respectively the equivalent complex gains of the Duffing nonlinearity, of the electrostatic nonlinearity and of the actuation nonlinearity. Straightforward integration leads to the following expressions:

$$N_{Duff}(A)=\frac{3}{4}\gamma A^2, \qquad (26)$$

and

$$N_{pulse}(A,\omega)=-j\frac{2\omega}{\pi A}f_p. \qquad (27)$$

One can directly compute an approximation of $N_{soft}(A)$, without passing through the intermediate step of (16)[2]. This yields:

$$N_{soft}(A,\omega)=-\delta\frac{\omega}{\pi}\int_0^{2\pi/\omega}I(A\sin(\omega t))\sin(\omega t)\exp(j\omega t)dt\approx-\delta\frac{1+\kappa A^2}{1-A^2}, \qquad (28)$$

where $\kappa\approx 0.182$ (cf. appendix A).

The Barkhausen criterion (22) then becomes:

$$\frac{3}{4}\gamma A^2-\delta\frac{1+\kappa A^2}{1-A^2}-j\frac{2\omega}{\pi A}f_p=\omega^2-1-j\frac{\omega}{Q}. \qquad (29)$$

There exists one unique couple (A_{osc},ω_{osc}) that cancels out the real part and the imaginary part of (29):

---

[2] There is little point in using $\hat{I}(a)$ to derive an analytical expression of $N_{soft}(A)$: this approach leads to an expression involving elliptic integrals which can only be apprehended with difficulty (and should then be approximated, leading to a simpler but less accurate expression which would be an approximation of an approximation).

$$\begin{cases} A_{osc} = \dfrac{2}{\pi} f_p Q \\ \omega_{osc} = \left(1 + \dfrac{3}{4} \gamma A_{osc}^2 - \delta \dfrac{1 + \kappa A_{osc}^2}{1 - A_{osc}^2} \right)^{1/2} \end{cases} . \quad (30)$$

The values that may be taken by A_{osc} are theoretically limited by the second equation, i.e. there can be no oscillation regime such that $A_{osc} > A_{\max}$, where $A_{\max}$ satisfies:

$$1 + \frac{3}{4} \gamma A_{\max}^2 - \delta \frac{1 + \kappa A_{\max}^2}{1 - A_{\max}^2} = 0 , \quad (31)$$

for which $\omega_{osc} = 0$. However, one should not expect this limit to have a practical importance: first of all, in many practical cases $a_{\max} < A_{\max}$: this is typically the case when $\gamma > 0$ (hardening Duffing behavior) and $0 < \delta < 1$. Thus, the electrostatic instability discussed in section 3.2 sets a tighter limit on the oscillation amplitude than (31). Moreover, as we have already mentioned, DFA accurately predicts the behavior of systems that satisfy the filter hypothesis: it is clear that, if ω_{osc} decreases sufficiently, the high-order harmonics generated by the different nonlinearities are no longer filtered out by the linear part and the filter hypothesis holds no more. Thus, the value of $A_{\max}$ that can be inferred from (31) is out of the range of validity of DFA. This shows that one should be very careful when trying to determine the onset of electrostatic instability under sinusoidal motion assumptions [16-17], because the two notions (instability and sinusoidal motion) are somehow contradictory. This is confirmed by a stability analysis based on DFA: the oscillatory regime defined by (30) is stable provided (24) is satisfied. We have:

$$\left. \frac{\partial \mathrm{Im}}{\partial \omega} \right|_{\substack{A_{osc} \\ \omega_{osc}}} = 0 , \left. \frac{\partial \mathrm{Re}}{\partial \omega} \right|_{\substack{A_{osc} \\ \omega_{osc}}} = -2\omega_{osc} \text{ and } \left. \frac{\partial \mathrm{Im}}{\partial A} \right|_{\substack{A_{osc} \\ \omega_{osc}}} = \frac{\omega_{osc}}{A_{osc} Q} , \quad (32)$$

thus the stability condition boils down to:

$$\frac{\omega_{osc}^2}{A_{osc} Q} > 0 \Leftrightarrow \omega_{osc}^2 > 0 , \quad (33)$$

which is always satisfied. However, we have shown in section 3 that the amplitude of the oscillations of a pulse-actuated structure cannot exceed $a_{\max}$. Thus the resonant stability condition is simply:

$$A_{osc} \le a_{\max} . \quad (34)$$

It is interesting to study the dependency of ω_{osc} on A_{osc}. It is notable that, depending on the system's parameters, there may exist an optimal value of $A_{osc} \le a_{\max}$ for which

$$\frac{d\omega_{osc}}{dA_{osc}} = 0 . \quad (35)$$

This value is "optimal" in the sense that small variations of the amplitude will not affect the value of ω_{osc}: thus, one may achieve large amplitude oscillations *and* good frequency stability, both of which would be very desirable features in MEMS/NEMS reference oscillator applications [18-19].

4.3. Describing function analysis of the open-loop system

Before moving on to the comparison of these results with simulated data, we stress the fact that the existence and the uniqueness of a stable periodic regime for an electrostatic pulse-actuated clamped-clamped beam are only valid when the system is operated in closed-loop, and in particular when the pulses are triggered when the detected signal crosses zero.

A simplified model of the open-loop beam is represented in figure 5[3]. In this configuration, there may exist up to five oscillation states at a given excitation amplitude and pulsation: this can be inferred from the DFA of (11), where one assumes that $a = A\sin(\omega t + \varphi)$ (the fact that the loop is open no longer ensures that a is in phase with the excitation) and the origin of time coincides with a positive pulse. Projecting this equation on $\exp(j\omega t)$ yields, after using (28):

$$\left[\left(1+\frac{3}{4}\gamma A^2 - \delta\frac{1+\kappa A^2}{1-A^2} - \omega^2\right) + j\frac{\omega}{Q}\right]A = \omega\frac{2}{\pi}f\left(\sin\varphi + j\cos\varphi\right), \qquad (36)$$

where f is the amplitude of the Dirac pulses injected into the system.

Taking the squared modulus of (36) results, after multiplication by $\left(1-A^2\right)^2$, in a fifth-order polynomial in A^2:

$$\begin{aligned}
&\frac{9}{16}\gamma^2 A^{10} + \frac{3}{2}\gamma\left(1-\frac{3}{4}\gamma + \delta\kappa - \omega^2\right)A^8 \\
&+\left(\frac{9}{16}\gamma^2 - \frac{3}{2}\gamma\left(2-\delta(1-\kappa)\right) + (1+\delta\kappa)^2 + \left(\frac{3}{2}\gamma + \frac{1}{Q^2} - 2\left(1-\frac{3}{4}\gamma+\delta\kappa\right)\right)\omega^2 + \omega^4\right)A^6 \\
&+\left(2(1-\delta)\left(1-\frac{3}{4}\gamma+\delta\kappa\right) - \left(\frac{4f^2}{\pi^2} + \frac{2}{Q^2} - 2(1-\delta) - 2\left(1-\frac{3}{4}\gamma+\delta\kappa\right)\right)\omega^2 - 2\omega^4\right)A^4 \\
&+\left((1-\delta)^2 + \left(2\delta - 2 + \frac{8f^2}{\pi^2} + \frac{1}{Q^2}\right)\omega^2 + \omega^4\right)A^2 - \frac{4f^2\omega^2}{\pi^2} = 0
\end{aligned} \qquad (37)$$

This polynomial may have multiple roots, meaning that the open-loop system may have up to five oscillation states[4] and exhibit hysteretic behavior. The corresponding values of φ are given by:

$$\tan\varphi = \frac{Q}{\omega}\left[\left(1+\frac{3}{4}\gamma A^2 - \delta\frac{1+\kappa A^2}{1-A^2}\right) - \omega^2\right]. \qquad (38)$$

Closing the loop simply ensures that φ takes a specific value (in our case, $\varphi = 0$) and, thus, results in a single possible oscillation state (figure 6).

The case when the sensor is operated in closed-loop in the presence of phase-delay (consequent to the filtering of the detected signal) between the pulses and the triggering event is the subject of forthcoming work. The fundamental difference between these cases and the zero-phase delay case covered in the present work is that the amplitude of the pulses is modulated by the electrostatic nonlinearity: for large values of the phase-delay, this may result in multiple oscillation states, even though the loop is closed.

6. Simulation and results

The purpose of this section is to validate with simulations the theoretical results obtained in the previous sections. This validation is conducted in two steps: first, the validity of the describing function approach is demonstrated by simulating the one-degree-of-freedom model (11), in which $I(a)$ is replaced by $\hat{I}(a)$ (16) and the pulses have finite duration. A more complex model, obtained by projecting (8) on three eigenmodes, is then simulated to verify the well-foundedness of the simpler model (11). The parameters of the resonator correspond to those of the accelerometer structure (figure 7) developed in the ANR-funded M&NEMS project: L=25µm, b=500nm, $h = G$=250nm, Q=6000, ρ=2320kg.m^{-3}, E=149GPa. For this set of parameters, $\omega_0 \approx 2.07\times10^7$rad.s^{-1},

[3] It is simplified in the sense that, in the system represented in figure 1, the amplitude of the pulses of electrostatic force depends on the value of the phase-delay, as can be inferred from (2).

[4] When $\delta = 0$, up to three oscillation states may be observed. This corresponds to the well-known 'critical amplitude' phenomenon associated with the Duffing pendulum [9].

$V_{pi} \approx 29.63\text{V}$, $\gamma \approx 0.719$. In the actual circuit, the duration of the impulses is set to $T_p = 10\text{ns}$ ($\tau_p = 0.207$), so that they may be considered short with respect to the period of oscillation. The bias voltage that is applied to the structure is equal to the maximum supply voltage of the technology chosen for the circuit -in the present case, ST CMOS 130 nm- i.e. $V_b = 1.2\text{V}$, which corresponds to $\delta \approx 1.64 \times 10^{-3}$.

Solving (19), we find that the pull-in amplitude is $a_{\max} \approx 0.995$. From (30) and (15), the beam should not be pulled-in, provided $f_p < 2.59 \times 10^{-4}$, i.e. $V_p < 0.346\,\text{V}$.

6.1 Simulation of the 1-DOF model

The transient simulation of (11) is conducted with Matlab/Simulink. In this environment, the pulsed force necessarily has a finite duration τ_p, which introduces a small amount of phase delay into the feedback loop. To determine the influence of this non-ideality, two sets of simulations are run: one with $\tau_p = 0.207$, the other with $\tau_p = 0.0207$. The oscillation amplitude and the oscillation pulsation are determined at the end of the simulation, when the steady-state regime has supposedly been reached. In theory, the amplitude and the pulsation should behave according to (30), as depicted in figure 8. The relative error between simulation and theory is represented in figure 9. As anticipated, the error increases with τ_p. However, the agreement is very good, even for "long" pulses, with relative errors inferior to 4% for the amplitude and inferior to 2% for the pulsation, even when the oscillation amplitude is very close to 1. This validates the describing function approach of section 5. Moreover, we verify that the beam pulls-in when the oscillation amplitude becomes larger than $a_{\max} \approx 0.995$.

6.2 Simulation of the 3-DOF model

A less idealized model is simulated: (8) is decomposed and projected on the first three relevant eigenmodes of the beam. The projection integrals are evaluated at each integration step with a first-order Newton-Cotes quadrature scheme. τ_p-long pulses are triggered when the total charge accumulated on the beam crosses zero. The charge is calculated at every time-step by integrating (5) along the length of the beam. The oscillation amplitude is defined as the maximal displacement amplitude of the midpoint of the beam and the oscillation period is calculated as the difference between two consecutive zero-crossings of the total charge. The errors have the same orders of magnitude as for the 1-DOF model and the same behaviour with respect to τ_p. This validates the use of (30) to predict the behaviour of the actual system. However, some qualitative differences do exist between the 1-DOF case and the 3-DOF case, as illustrated in figure 10. Furthermore, the beam is pulled in at $a_{\max} \approx 0.982$ for $\tau_p = 0.207$ and at $a_{\max} \approx 0.990$ for $\tau_p = 0.0207$. Thus, for large oscillation amplitudes, the second and third modes have a small (but finite) contribution to the elastic energy of the system: it is difficult to derive general results from these simulations without resorting to finer, more complex, models than those developed in section 5. For example, using DFA makes it impossible to predict sub-harmonic resonances that are likely to appear in low-frequency open-loop excitation contexts (more appropriate methods are described in [20]). The case of inter-mode crosstalk may be addressed if simplifying assumptions are made (for example, if all the modes oscillate in phase).
The system was simulated for several other sets of parameters, in closed-loop as well as in open-loop, resulting in very small errors between theory and simulation, as long as the hypotheses made in section 5 were respected.

7. Conclusion

In this paper, we have shown that very simple closed-loop control schemes can be used to achieve stable large-amplitude motion of a resonant structure, even when jump resonance (caused by electrostatic softening or Duffing hardening) is present in its open-loop frequency response. The case of a capacitive pulse-actuated resonant accelerometer sensing cell was thoroughly investigated.
The nonlinear softening term was approximated with simple expressions, valid across the whole gap. This helped us establish the maximal displacement amplitude $a_{\max}$ that can be achieved by a closed-loop pulse-actuated

clamped-clamped beam without incurring electrostatic instability: it was shown that, depending on the structure's design parameters γ and δ, almost full-gap travel range is possible. The same approach may also be used for other beam-electrode configurations or for other actuation schemes. Using describing function analysis, we studied closed-loop and open-loop pulse-actuation and showed that the closed-loop approach ensures the stability of the motion of the beam even when the open-loop frequency response has a hysteretic characteristic. Some analytical expressions of the oscillation amplitude and of the oscillation pulsation were established and validated with transient simulations of the nonlinear closed-loop system, in the case of the sensing cell of the ANR-funded M&NEMS project.

The most immediate practical consequence of the present work is that, with proper mechanical and feedback design, very large oscillation amplitudes and, thus, signal-to-noise ratios may be achieved, thereby relaxing the constraints on the design of the analog front-end of the electronic circuitry. Another practical consequence is that, as mentioned in section 5, the softening nonlinearity can be used to compensate for the hardening nonlinearity to achieve large oscillation amplitudes together with good frequency stability [18].

The analysis of the closed-loop system when phase-delay is present in the feedback loop is the subject of ongoing work. Furthermore, an ASIC implementing the electrostatic actuation and detection scheme described in this paper has been developed and should soon be tested.

Appendix A

Equation (16) is obtained by fitting the projection of the electrostatic force on the first eigenmode with a two parameter model parameterized by $\hat{n}_0$ and $\hat{\kappa}_0$. Let us then define

$$\{\hat{n}_\varepsilon, \hat{\kappa}_\varepsilon\} = \arg\min_{n,\kappa} \int_0^{(1-\varepsilon)} \left[\frac{1+\kappa a^2}{(1-a^2)^n} - I(a) \right]^2 da, \qquad \text{(A-1)}$$

where

$$I(a) = \left(\int_0^1 \frac{{w_0}^2}{\left(1-a^2 {w_0}^2\right)^2} d\tilde{x} \right) \Bigg/ \left(\int_0^1 {w_0}^2 d\tilde{x} \right), \qquad \text{(A-2)}$$

so that, on $[0, 1-\varepsilon]$, the quadratic distance between $I(a)$ and the model $\hat{I}(\hat{n}_\varepsilon, \hat{\kappa}_\varepsilon, a)$ is minimal. Replacing the integrals appearing in the cost function with numerical approximations, it is possible to use the Gauss-Newton algorithm, for example, to find $\hat{n}_\varepsilon$ and $\hat{\kappa}_\varepsilon$ for different values of ε. The values of $\hat{n}_0$ and $\hat{\kappa}_0$ are then calculated with an extrapolation method as the limits of sequences $\hat{n}_\varepsilon$ and $\hat{\kappa}_\varepsilon$. This leads to $\hat{n}_0 \approx 1.500$ and $\hat{\kappa}_0 \approx -0.041$: the corresponding relative error is smaller than 1% across the whole gap (figure A1) and close to 0% for $a \approx 1$. However, using $\hat{n}_0 = 1.5$ and $\hat{\kappa}_0 = 0$ also yields good results and leads to simpler analytical developments.

The same approach can be used to determine an approximation of $N_{soft}(A)$ except one must now minimize:

$$\int_0^{(1-\varepsilon)} \left[\frac{1+\kappa a^2}{(1-a^2)^n} - J(a) \right]^2 da, \qquad \text{(A-3)}$$

where

$$J(a) = \frac{1}{\pi} \int_0^{2\pi} I(A\sin(t))\sin^2(t) dt. \qquad \text{(A-4)}$$

We find $\hat{n}_0 \approx 1.004$ and $\hat{\kappa}_0 \approx 0.182$. One may round $\hat{n}_0$ to 1 and $\hat{\kappa}_0$ to 0.182 without deteriorating the results (a relative error of less than 2% for $a = 0.99$, figure A1). Choosing a slightly smaller value of $\hat{\kappa}_0$ (say, $\hat{\kappa}_0 = 0.160$) yields a better approximation for moderate values of a, whereas a larger value of $\hat{\kappa}_0$ ($\hat{\kappa}_0 = 0.221$) improves the accuracy at very large amplitudes but reduces it for moderate a (figure A2). Any value of $\hat{\kappa}_0$ in the range $[0.160, 0.221]$ ensures that the relative error is smaller than 5% across the whole gap.

The fact that $\hat{\kappa}_0 = 0.221$ yields the best results for $a \approx 1$ can be explained analytically. Starting from $\hat{I}(1.5,-0.041,a)$, which minimizes (A-1), one may find a closed-form expression (involving complete elliptic integrals, as mentioned in section 4) of the corresponding describing function gain. In the neighborhood of $a = 1$, this gain behaves as:

$$\frac{K}{1-a^2},\ K = \frac{4}{\pi}(1-0.041) \approx 1.221. \qquad \text{(A-5)}$$

Since $\hat{I}(1.5,-0.041,a)$ is a good approximation of $I(a)$ in the neighborhood of $a = 1$ (figure A1), one may then expect $\frac{1+0.221a^2}{1-a^2}$ to be a good approximation of $J(a)$ in the same region, as is indeed the case (figure A2).

It should be mentioned that the same approach can be used when the length of the electrode is smaller than L. However, the resulting values of $\hat{n}_0$ are no longer integers or half-integers (except when the length of the electrode goes to zero) and, as a consequence, determining the pull-in voltage or the open-loop response of the system does not boil down to finding the roots of low-order polynomials.

References

[1] Stemme G, "Resonant silicon sensors", *Journal of Micromechanics and Microengineering*, vol. 1, n. 2, 1991, pp. 113-125

[2] Roessig T, "Integrated MEMS tuning fork oscillators for sensor applications," Ph.D. dissertation, Department of Mechanical Engineering, University of California, Berkeley, 1998

[3] Ekinci K L, Yang Y T, Roukes M L, "Ultimate limits to inertial mass sensing based upon nanoelectromechanical systems", *Journal of Applied Physics*, vol. 95, n. 5, 2004, pp. 2682-2689

[4] Gallacher B J, Burdess J S, Harish K M, "A control scheme for a MEMS electrostatic resonant gyroscope excited using combined parametric excitation and harmonic forcing", *Journal of Micromechanics and Microengineering*, vol. 16, n. 2, 2006, pp. 320-331

[5] Sung S, Lee J G, Lee B, Kang T, "Design and performance test of an oscillation loop for a MEMS resonant accelerometer", *Journal of Micromechanics and Microengineering*, vol. 13, n. 2, 2003, pp. 246-253

[6] Ahn Y, Guckel H, Zook J D, "Capacitive microbeam resonator design", *Journal of Micromechanics and Microengineering*, vol. 11, n. 1, 2001, pp. 70-80

[7] Colinet E, Juillard J, Guessab S, Kielbasa R, "Actuation of resonant MEMS using short pulsed forces", *Sensors and Actuators A*, vol. 115, n. 1, 2004, pp. 118-125

[8] Juillard J, Bonnoit A, Avignon E, Hentz S, Kacem N, Colinet E, "From MEMS to NEMS: closed-loop actuation of resonant beams beyond the critical Duffing amplitude", 2008 IEEE Sensors, p 510-13, 2008

[9] Kaajakari V, Mattila T, Oja A, Seppä H, "Nonlinear limits for single-crystal silicon microresonators", *Journal of Microelectromechanical Systems*, vol. 13, n. 5, 2004, pp.715-724

[10] Lifshitz R, Cross M C, "Nonlinear dynamics of nanomechanical and micromechanical resonators", *Review of Nonlinear Dynamics and Complexity*, vol. 1, 2008, pp. 1-52

[11] Leus V, Elata D, "On the Dynamic Response of Electrostatic MEMS Switches", *Journal of Microelectromechanical Systems*, vol. 17, n. 1, 2008, pp. 236-243

[12] Nielson G N, Barbastathis G, "Dynamic pull-in of parallel-plate and torsional electrostatic MEMS actuators", *Journal of Microelectromechanical Systems*, vol. 15, n. 4, 2006, pp.811-821

[13] Colinet E *et al.*, "Ultra-Sensitive Capacitive Detection Based on SGMOSFET Compatible With Front-End CMOS Process", *IEEE Journal of Solid-State Circuits*, vol. 47, n. 1, 2009, pp. 247-257

[14] Chow S N, Hale J K, "Methods of Bifurcation Theory", Springer-Verlag, Berlin, 1982

[15] Gelb A, Van der Velde W, "Multiple-input describing functions and nonlinear system design", McGraw-Hill, New-York, 1968

[16] Kacem N, Hentz S, Pinto D, Reig B, Nguyen V, "Nonlinear dynamics of nanomechanical beam resonators: improving the performance of NEMS-based sensors", Nanotechnology, vol. 20, 2009, 11pp.

[17] Fargas-Marques A, Casals-Terré J, Shkel A M, "Resonant pull-in condition in parallel-plate electrostatic actuators", *Journal of Microelectromechanical Systems*, vol. 16, n. 5, 2007, pp. 1044-1053
[18] Juillard J, Arndt G, Colinet E, "Enhancing the frequency stability of a NEMS oscillator with electrostatic and mechanical nonlinearities", Eurosensors 2009 (accepted)
[19] Kaajakari V, Koskinen J K, Mattila T, "Phase noise in capacitively coupled micromechanical oscillators", *IEEE Transactions on Ultrasonics, Ferroelectrics, and Frequency Control*, vol. 52, n. 12, 2005, pp. 2322-2331
[20] Abdel-Rahman E M, Nayfeh A H, "Secondary resonances of electrically actuated resonant microsensors", *Journal of Micromechanics and Microengineering*, vol. 13, n. 3, pp. 491-501

Figure captions

Figure 1. Top-view of the mechanical structure (a) (not to scale) and diagram of the closed-loop actuation and detection scheme (b).

Figure 2. Typical aspect of $E_{pot}(a)$ when $\delta < 1$ (left) and when $\delta \geq 1$ (right).

Figure 3. $a_{\max}$ vs. δ, for different values of γ. The plain black curve corresponds to (20).

Figure 4. Block-diagram representation of the capacitive pulse-actuated clamped-clamped beam, operated in closed-loop.

Figure 5. Block-diagram representation of the capacitive pulse-actuated clamped-clamped beam, operated in open-loop.

Figure 6. Amplitude (top) and phase (bottom) frequency response of the open-loop system, with $\gamma = 0.5$, $\delta = 0.1$, $Q = 100$ and $f = 2 \times 10^{-3}$ (a), $f = 4 \times 10^{-3}$ (b), $f = 8 \times 10^{-3}$ (c), $f = 12 \times 10^{-3}$ (d). The continuous line represents $a_{\max}$ and the black circle corresponds to the system's self oscillation regime, defined by $\varphi = 0$. As the force increases, the system goes from linear to doubly-hysteretic.

Figure 7. SEM of one of the accelerometer structures developed in the M&NEMS project.

Figure 8. ω_{osc} vs. A_{osc}, as predicted by (30). The relationship between A_{osc} and f is linear.

Figure 9. Relative error on the values of A_{osc} and ω_{osc} predicted by (30) and obtained by simulation of the 1-DOF model.

Figure 10. Relative error on the values of A_{osc} and ω_{osc} predicted by (30) and obtained by simulation of the 3-DOF model.

Figure A1. $I(a)$ (top left), $J(a)$ (top right) and relative errors (bottom) vs. amplitude.

Figure A2. Relative error between $J(a)$ and $\hat{J}(n_0, \kappa_0, a)$, for different values of $\hat{\kappa}_0$.

(a)

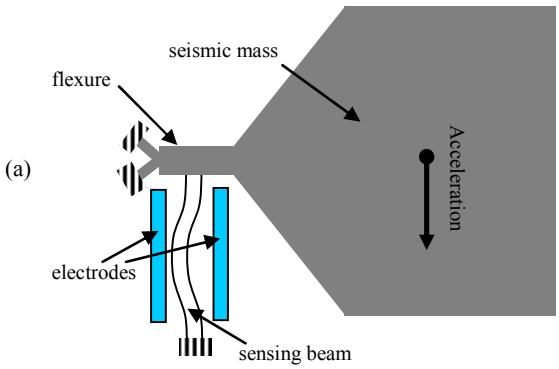
seismic mass
flexure
Acceleration
electrodes
sensing beam

(b)

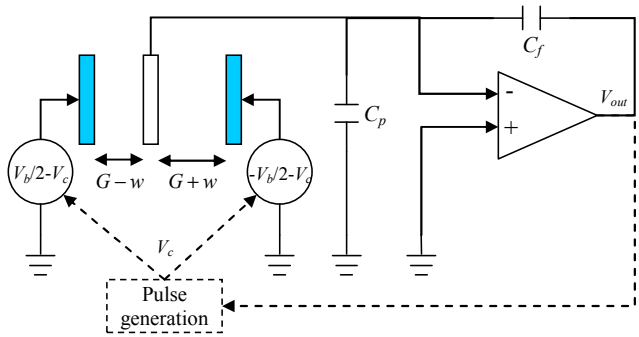
C_f
V_{out}
C_p
$V_b/2\text{-}V_c$
$G-w$
$G+w$
$-V_b/2\text{-}V_c$
V_c
Pulse generation

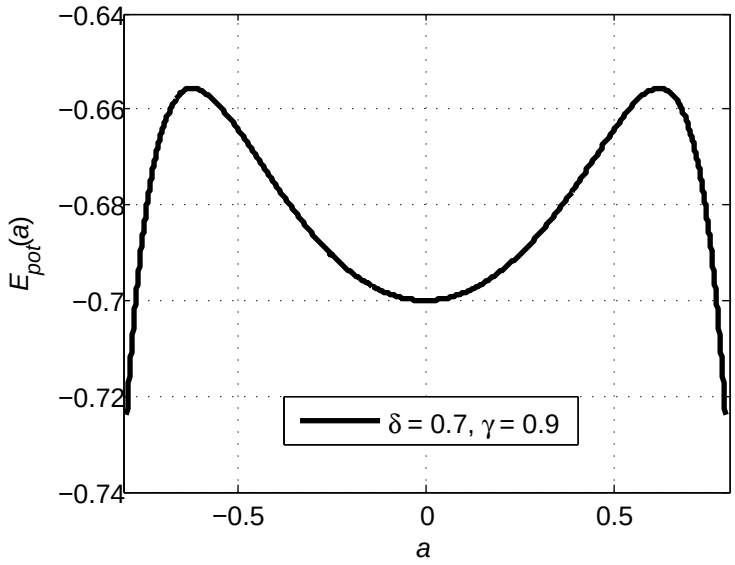
−0.64
−0.66
−0.68
−0.7
−0.72
−0.74
$E_{pot}(a)$
−0.5
0
0.5
a
δ = 0.7, γ = 0.9

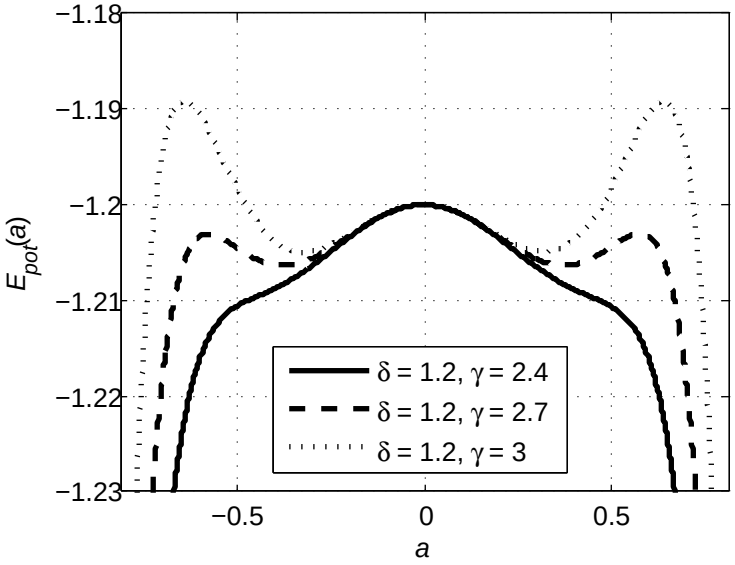
−1.18
−1.19
−1.2
−1.21
−1.22
−1.23
$E_{pot}(a)$
−0.5
0
0.5
a
δ = 1.2, γ = 2.4
δ = 1.2, γ = 2.7
δ = 1.2, γ = 3

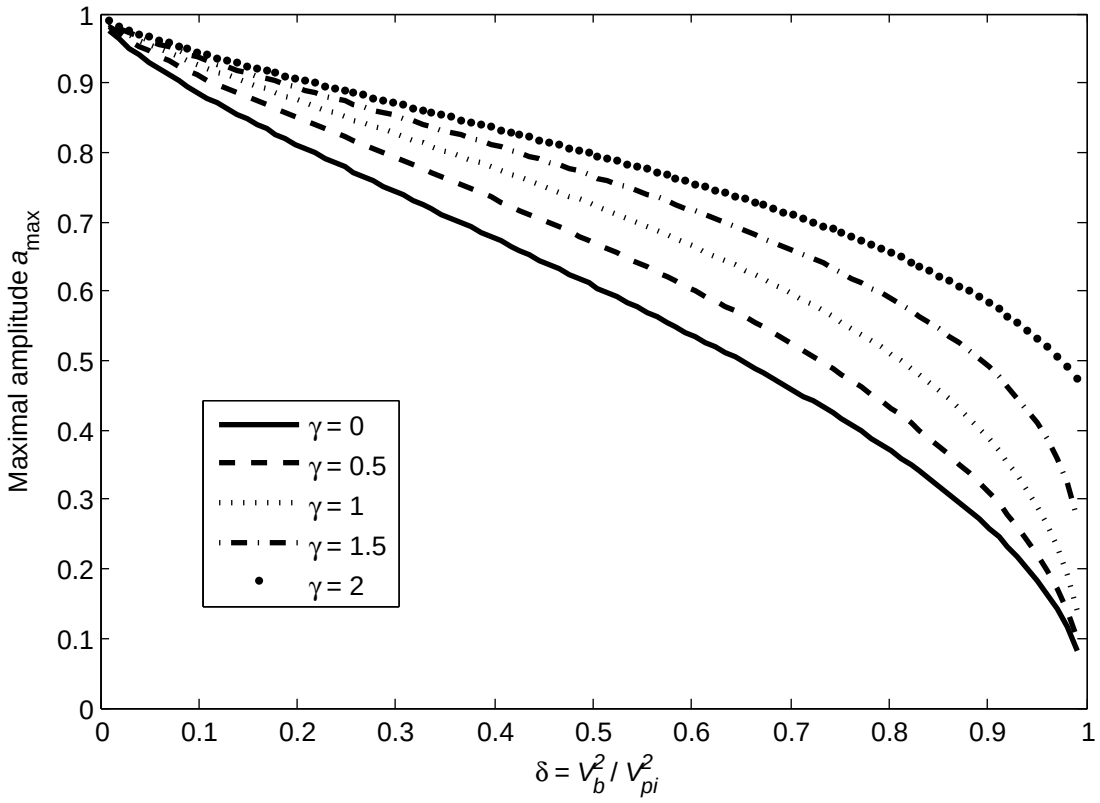
Maximal amplitude a_{max}
$\delta = V_b^2 / V_{pi}^2$
γ = 0
γ = 0.5
γ = 1
γ = 1.5
γ = 2
0
0.1
0.2
0.3
0.4
0.5
0.6
0.7
0.8
0.9
1

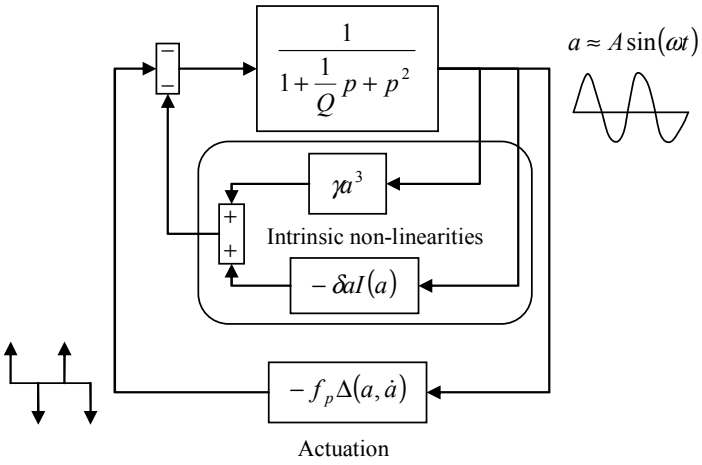
$\frac{1}{1+\frac{1}{Q}p+p^2}$
$a \approx A\sin(\omega t)$
γa^3
Intrinsic non-linearities
$-\delta a I(a)$
$-f_p\Delta(a,\dot{a})$
Actuation

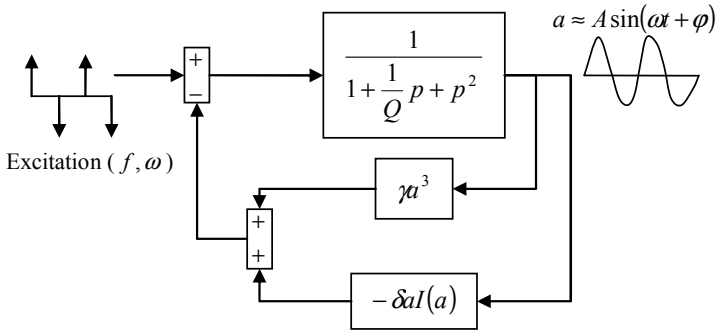
$a \approx A\sin(\omega t + \varphi)$
$\frac{1}{1+\frac{1}{Q}p+p^2}$
Excitation (f, ω)
γa^3
$-\delta a I(a)$

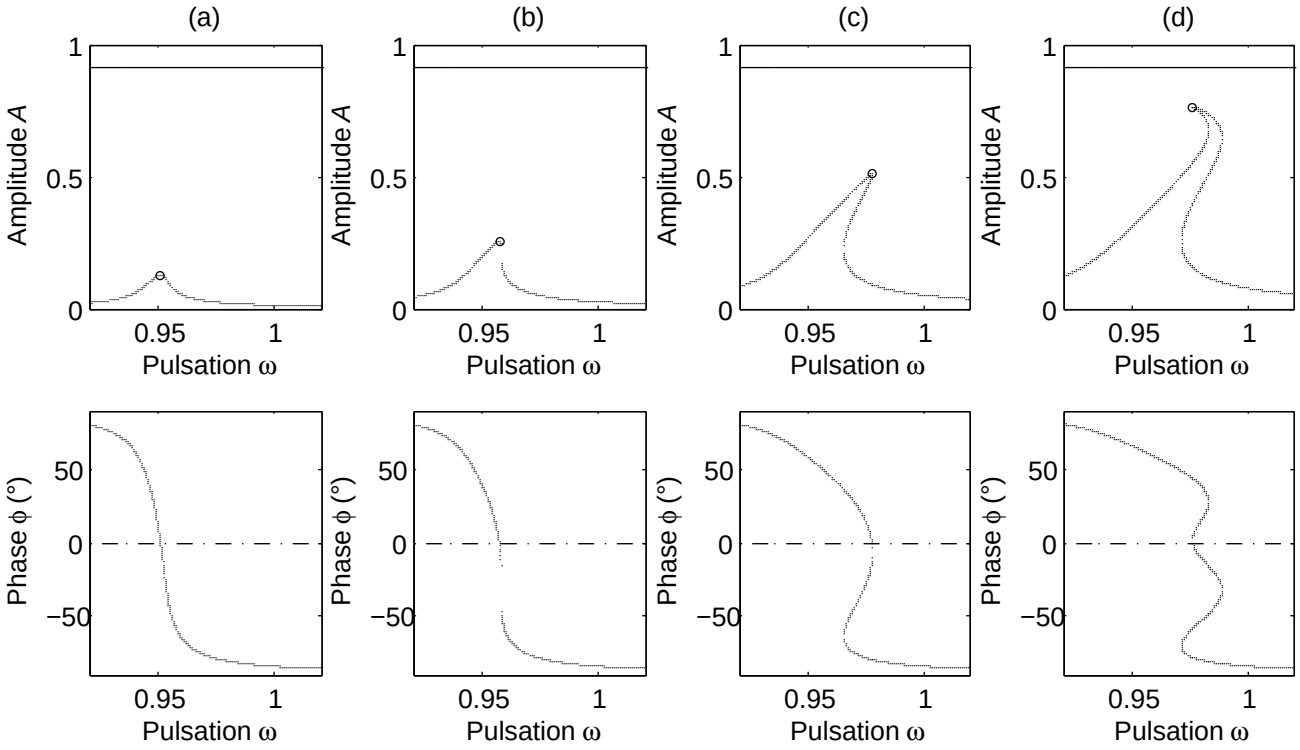
(a)
(b)
(c)
(d)
Amplitude A
Phase ϕ (°)
Pulsation ω
1
0.5
0
50
−50
0.95

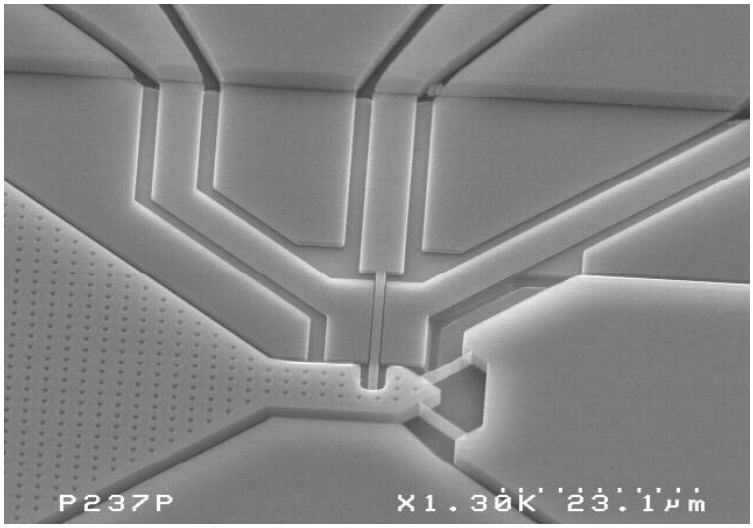
P237P
X1.30K 23.1µm

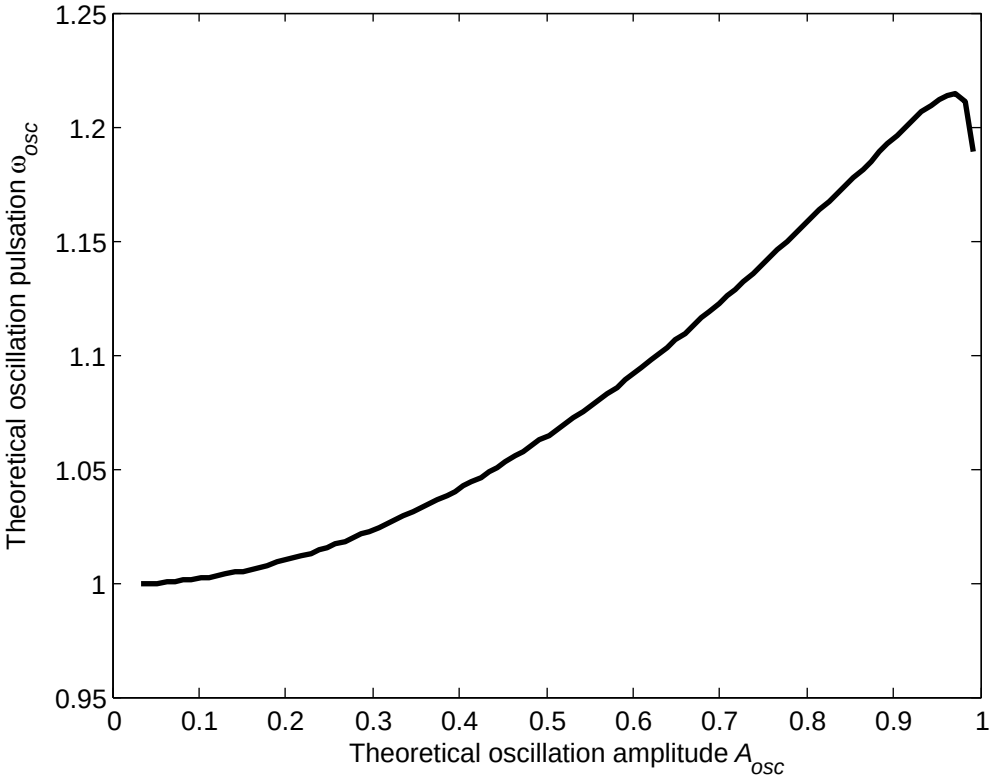
1.25
1.2
1.15
1.1
1.05
1
0.95
0
0.1
0.2
0.3
0.4
0.5
0.6
0.7
0.8
0.9
1
Theoretical oscillation pulsation ω_osc
Theoretical oscillation amplitude A_osc

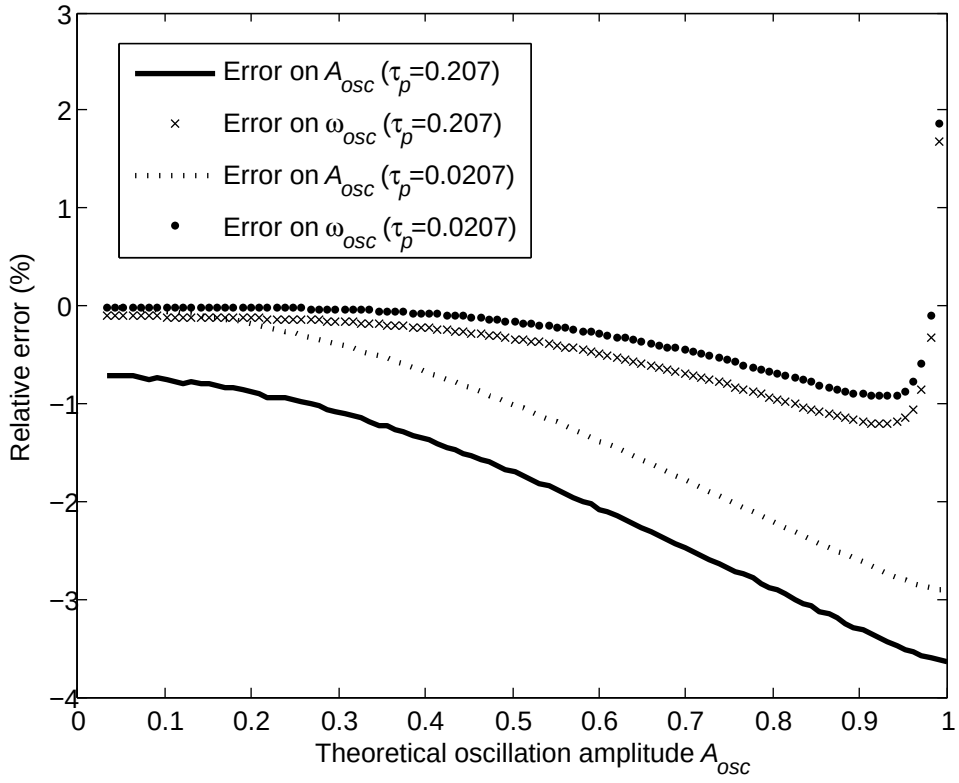
Error on A_{osc} (τ_p=0.207)
Error on ω_{osc} (τ_p=0.207)
Error on A_{osc} (τ_p=0.0207)
Error on ω_{osc} (τ_p=0.0207)
Relative error (%)
Theoretical oscillation amplitude A_{osc}
3
2
1
0
−1
−2
−3
−4
0
0.1
0.2
0.3
0.4
0.5
0.6
0.7
0.8
0.9
1

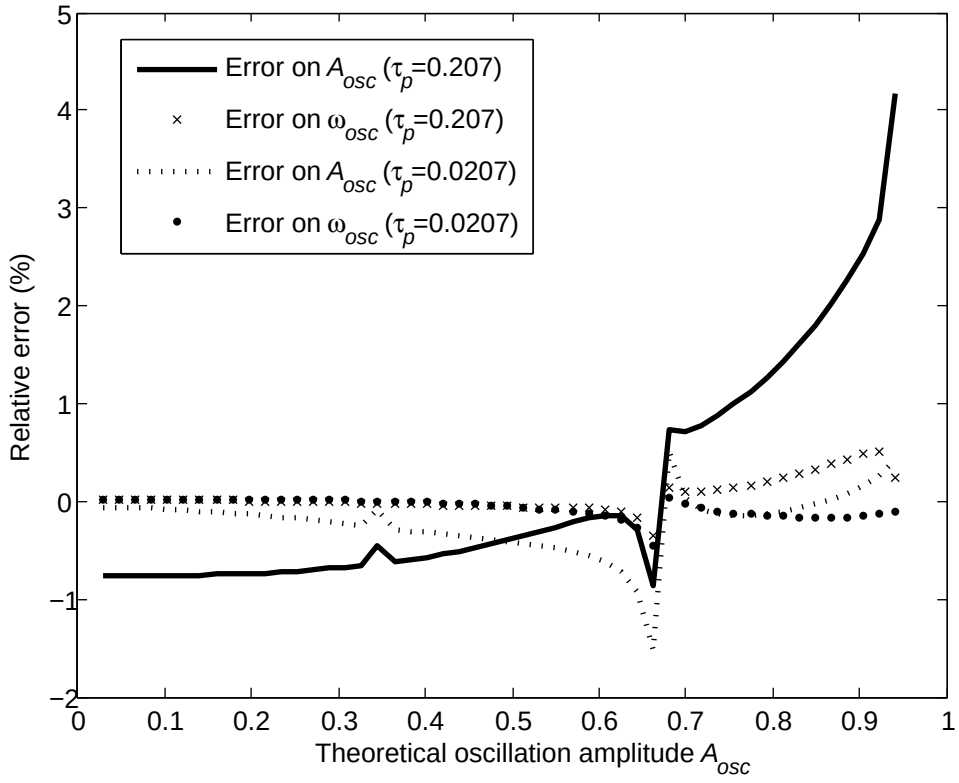
Error on A_{osc} (τ_p=0.207)
Error on ω_{osc} (τ_p=0.207)
Error on A_{osc} (τ_p=0.0207)
Error on ω_{osc} (τ_p=0.0207)
Relative error (%)
Theoretical oscillation amplitude A_{osc}
5
4
3
2
1
0
−1
−2
0
0.1
0.2
0.3
0.4
0.5
0.6
0.7
0.8
0.9
1

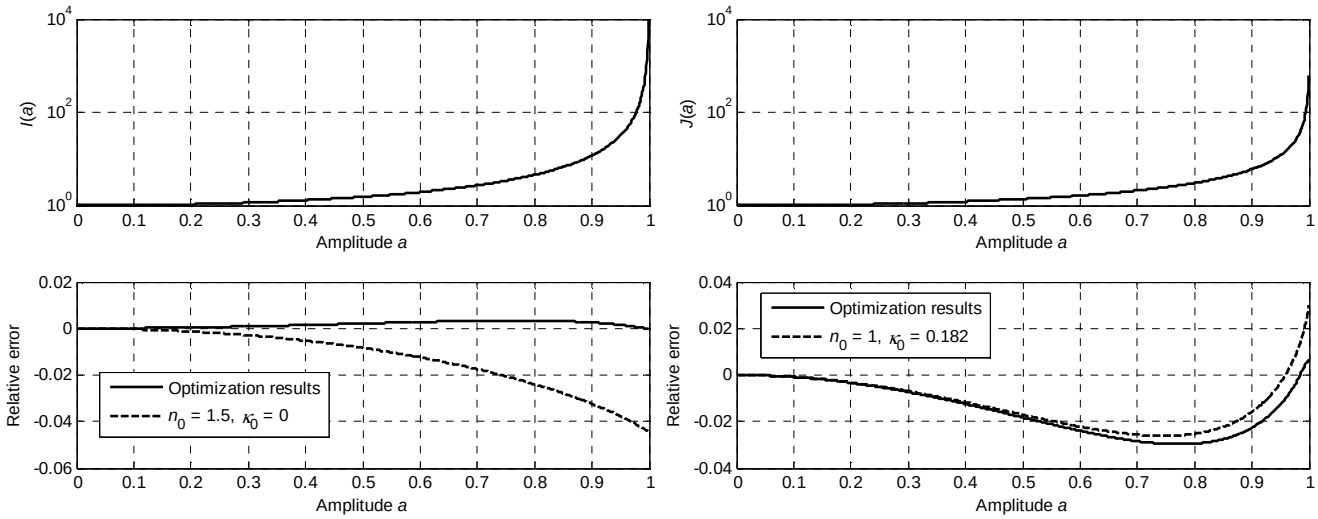
10^4
10^2
10^0
$I(a)$
0 0.1 0.2 0.3 0.4 0.5 0.6 0.7 0.8 0.9 1
Amplitude a
10^4
10^2
10^0
$J(a)$
0 0.1 0.2 0.3 0.4 0.5 0.6 0.7 0.8 0.9 1
Amplitude a
0.02
0
-0.02
-0.04
-0.06
Relative error
Optimization results
n_0 = 1.5, κ_0 = 0
0 0.1 0.2 0.3 0.4 0.5 0.6 0.7 0.8 0.9 1
Amplitude a
0.04
0.02
0
-0.02
-0.04
Relative error
Optimization results
n_0 = 1, κ_0 = 0.182
0 0.1 0.2 0.3 0.4 0.5 0.6 0.7 0.8 0.9 1
Amplitude a

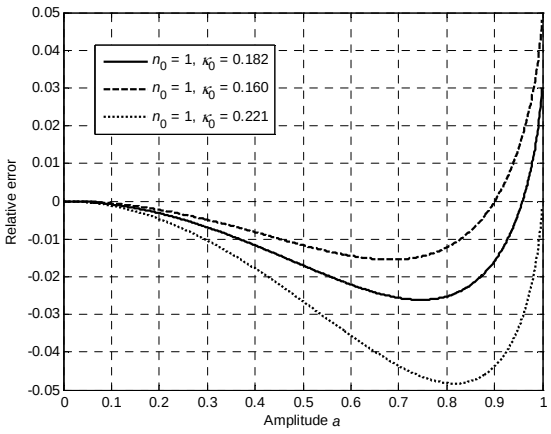
0.05
0.04
0.03
0.02
0.01
0
-0.01
-0.02
-0.03
-0.04
-0.05
Relative error
0
0.1
0.2
0.3
0.4
0.5
0.6
0.7
0.8
0.9
1
Amplitude a
n0 = 1, κ0 = 0.182
n0 = 1, κ0 = 0.160
n0 = 1, κ0 = 0.221